Biosensors and Bioelectronics 58 (2014) 395–402

Contents lists available at ScienceDirect

Biosensors and Bioelectronics

journal homepage: www.elsevier.com/locate/bios

A fast and simple label-free immunoassay based on a smartphone

Fabio Giavazzi [a,b,1], Matteo Salina [a,b,1], Erica Ceccarello [a,b], Andrea Ilacqua [a], Francesco Damin [c], Laura Sola [c], Marcella Chiari [c], Bice Chini [d], Roberto Cerbino [a], Tommaso Bellini [a,**], Marco Buscaglia [a,*]

[a] Dipartimento di Biotecnologie Mediche e Medicina Traslazionale, Università degli Studi di Milano, 20090 Segrate, Italy
[b] Proxentia S.r.l., 20135 Milano, Italy
[c] Istituto di Chimica del Riconoscimento Molecolare—C.N.R., 20131 Milano, Italy
[d] Istituto di Neuroscienze—C.N.R., 20129 Milano, Italy

ARTICLE INFO

Article history:
Received 19 December 2013
Received in revised form
14 February 2014
Accepted 27 February 2014
Available online 12 March 2014

Keywords:
Optical biosensor
Protein microarray
Immunoassay
Biomolecular detection
Reflective phantom interface
Point-of-care

ABSTRACT

Despite the continuous advancements in bio-molecular detection and fluidic systems integration, the realization of portable and high performance devices for diagnostic applications still presents major difficulties, mostly because of the need to combine adequate sensitivity with low cost of production and operational simplicity and speed. In this context, we propose a compact device composed of a smartphone and a custom-designed cradle, containing only a disposable sensing cartridge, a tiny magnetic stirrer and a few passive optical components. The detection principle is the previously proposed Reflective Phantom Interface that is based on measuring the intensity of light reflected by the surface of an amorphous fluoropolymer substrate, which has a refractive index very close to that of the aqueous sample solution and hosts various antibodies immobilized within spots. The reflectivity of dozens of spots is monitored in real time by the phone's camera using the embedded flash LED as the illumination source. We test the performance of the combined device targeting heterologous immunoglobulins and antigens commonly used as markers for diagnoses of hepatitis B and HIV. Target concentrations as low as a few ng/ml can be rapidly and robustly determined by comparing the rate of increase of the signal after the addition of the sample with that measured after the subsequent addition of a standard solution with known concentration. The features of the proposed system enable the realization of novel handheld biosensing devices suitable for those applications where multiple targets have to be rapidly detected even without the presence of trained personnel.

1. Introduction

The continuous development of novel bio-detection approaches, potentially suitable for integration into compact, automated handheld devices (Myers and Lee, 2008; Holford et al., 2012), provides a vision of a forthcoming paradigm shift in the field of medical diagnostics (Gubala et al., (2012)) and, more generally, in all fields currently relying on lab-based biochemical analysis (Kozma et al., (2013)). In this context, the availability of high performance imaging sensors coupled with large computational power embedded into current smartphone devices represents an unprecedented opportunity for developing fully functioning, compact and low-cost instruments, avoiding expensive customized hardware fabrication. In recent years, this approach has been employed to realize a number of smartphone-based devices, including portable bright field, dark field and fluorescence microscopy systems (Tseng et al., (2010); Zhu et al., (2011b)), fluorescent cytometry platforms (Zhu et al., (2011a)), and automatic analyzers for quantifying the fluorescence (Lee et al., (2011)) or the scattering (You et al., (2013)) of labeling agents. However, few solutions have exploited smartphone functionality to realize label-free biosensors, which do not require labeling of the analytes, thus minimizing, in principle, sample processing and simplifying measurement procedures. In Gallegos et al. (2013) the phone camera was turned into a spectrophotometer for detecting the wavelength shifts in a photonic crystal biosensor, whereas in Huang and Ugaz (2013) the electrochemical dissolution of a chromium layer measured by imaging was shown to depend on the specific solution composition.

All of the above mentioned systems rely on some custom-designed, mobile phone attachment that takes advantage of the embedded camera and, when applicable, holds the sample in the

* Corresponding author. Tel.: +39 02503 30352; fax: +39 02503 30365.
** Corresponding author. Tel.: +39 02503 30353; fax: +39 02503 30365.
E-mail addresses: tommaso.bellini@unimi.it (T. Bellini), marco.buscaglia@unimi.it (M. Buscaglia).
[1] These authors contributed equally to the study.

http://dx.doi.org/10.1016/j.bios.2014.02.077
0956-5663/

correct position. Generally, additional rather bulky external components are required, such as a proper illumination source or a pumping system, which complicate the development of truly portable designs. Moreover, the complexity of the required measurement procedures or of the particular sensing substrate employed prevents the realization of sensitive and simple assays based on low-cost disposable cartridges, suitable for large-scale diagnostic exams to be performed by untrained personnel.

Here we report the invention of a simple accessory, with less than 5 cm in depth, that transforms a smartphone into a portable biosensing device, enabling the parallel, label-free quantification of multiple markers in a few minutes and with minimum intervention of the operator. The detection method employed is the previously proposed Reflective Phantom Interface (RPI) (Giavazzi et al., 2013) that relies on the measurement of the intensity of light reflected by an interface with very low reflectivity in water ($\sim 10^{-5}$), therefore being almost invisible. The intrinsic simplicity of this approach is that it exploits the built-in LED and camera for the acquisition of the image of the light reflected by the sensing surface. The only component external to the phone that may require an electric supply, possibly a battery, is a tiny magnetic stirrer about 1 cm wide, which could be integrated into the main body of the device in a further engineering step. Using a cuvette-based, pre-assembled, disposable plastic cartridge, we demonstrate the performance of the system detecting fractions of nM of blood markers for HIV and Hepatitis B in serum.

2. Methods

2.1. The detection principle

In general, tiny amounts of material with a refractive index different from the surrounding medium can be easily observed by optical methods. The same principle applies if the surrounding medium is chemically heterogeneous, but has a homogenous index of refraction. Fluorinated polymer materials can be realized in order to have the same index of refraction as water, hence facilitating the optical detection of carbon-based compounds, which typically provide a substantially higher refractive index. In previous studies, we have exploited this concept with a twofold approach: (i) we used suspensions of nano-colloids made of fluorinated materials and estimated the amount of molecules adhering to their functionalized surfaces from the intensity of the scattered light (Ghetta et al., 2005; Prosperi et al., 2006; Morasso et al., 2010), and (ii) we proposed the RPI method (Giavazzi et al., 2013), which is based on the measurement of the intensity of the light reflected by a flat interface. Solution (i) is affected by possible limitations due to particle aggregation and very large area of the solid–liquid interface. Therefore, solution (ii) is highly preferable when dealing with multivalent interactions and very low analyte concentrations, typical properties of diagnostic markers. Accordingly, here we employ the RPI approach (ii) for the sensitive detection of antibodies and bio-markers. In this method, the interface hosts immobilized receptors while separating an aqueous solution from a solid, transparent material with a similar refractive index. In the appropriate conditions, the adhesion of molecules at this kind of interface causes an easily measurable increase in the intensity of reflected light, from which the amount of surface bound species can be estimated.

2.2. The device

The RPI approach has been previously demonstrated using a bench-top apparatus acquiring the light reflected by a perfluorinated plastic substrate iso-refractive with water (Hyflon® AD, an amorphous copolymer of tetrafluoroethylene, trademarked product of Solvay Specialty Polymers Italy) (Giavazzi et al., 2013). Basic components of the set-up were a collimated, thermally stabilized LED source (nominal wavelength of 625 nm, 14 nm FWHM bandwidth), a high resolution CCD camera, a magnetic stirrer and a system for the thermal stabilization of the sample. The optical set-up was designed to maximize the sensitivity of the RPI detection in a multiplex configuration: The LED light was expanded and collimated using a Köhler illumination scheme, providing an incident beam with high spatial uniformity and controlled divergence; and the collection optics allowed the formation of the image of the RPI surface on the CCD sensor with a suitable filtering, enabling the accurate selection of the light reflected in the specular direction. In this work we show that the same detection approach can be efficiently exploited using a minimal set-up based on an unmodified smartphone (Desire HD, HTC, Taiwan) combined with a simple custom-designed cradle hosting the measuring sample cell, a small magnetic stirrer and enabling the miniaturization of the optical layout required for the RPI detection. The device does not incorporate any temperature control system, and, in this configuration, the only external component necessary is the stirrer driver. The light emitted by the embedded, white light flash LED with a power of about 20 mW, is directed onto the bio-recognition surface and the reflected light is imaged by the backside illuminated CMOS sensor of the photo camera, having array size 3264×2448 and pixel size 1.4×1.4 μm. The optical and mechanical schemes of the combined device are shown in Fig. 1(a) and (b), respectively, and photographs are reported in Fig. 1(c) and (d). The optical design, described in Fig. 1(a), ensures the concomitant accurate selection of the reflected light and the high resolution imaging of the sensing surface. The LED light, partially collimated by the built-in converging lens is deviated, by means of a glass slab and a mirror, in order to impinge on the diagonal surface of a right angle prism made of Hyflon® AD, which is contained in the sample cuvette. The reflected light is then collected by an external close-up lens, spatially filtered and imaged on the camera sensor. The apertures along the optical path, including the small clear aperture of the smartphone camera lens, provide an effective spatial filtering of both the illumination and reflected beam, thus enabling an efficient rejection of the stray light. A polarizer placed on the reflection path also contributes to the reduction of background light. In fact, in this geometry the reflected light is strongly polarized because the angle of incidence is substantially coincident with the Brewster's angle.

The add-on assembly is composed of three parts made of black polyoxymethylene (Fig. 1(b)): The smartphone is inserted into a plastic holder with holes aligned with the LED and the camera detector positions; most of the optical elements are fitted in the sample cartridge holder attached to the smartphone holder; a mirror is encapsulated on the side of the cartridge holder by means of the third plastic part. In order to perform the measurement, the smartphone and the cartridge are inserted into the assembled cradle (Fig. 1(c)), the flash is turned on, and, exploiting the smartphone autofocus system, an optimized image of the sensing surface is obtained (Fig. 1(d)).

2.3. Surface preparation and execution of the measurement

Similarly to the previous study, the Hyflon® AD prism was coated with a multifunctional copolymer of dimethylacrylamide (DMA), N-acryloyloxysuccinimide (NAS), and 3-(trimethoxysilyl) propyl methacrylate (MAPS)–copoly(DMA-NAS-MAPS)—that both provides reactive groups for antibody immobilization and limits the unwanted nonspecific adsorption of serum components (Cretich et al., 2004). On the copolymer, different probe antibodies

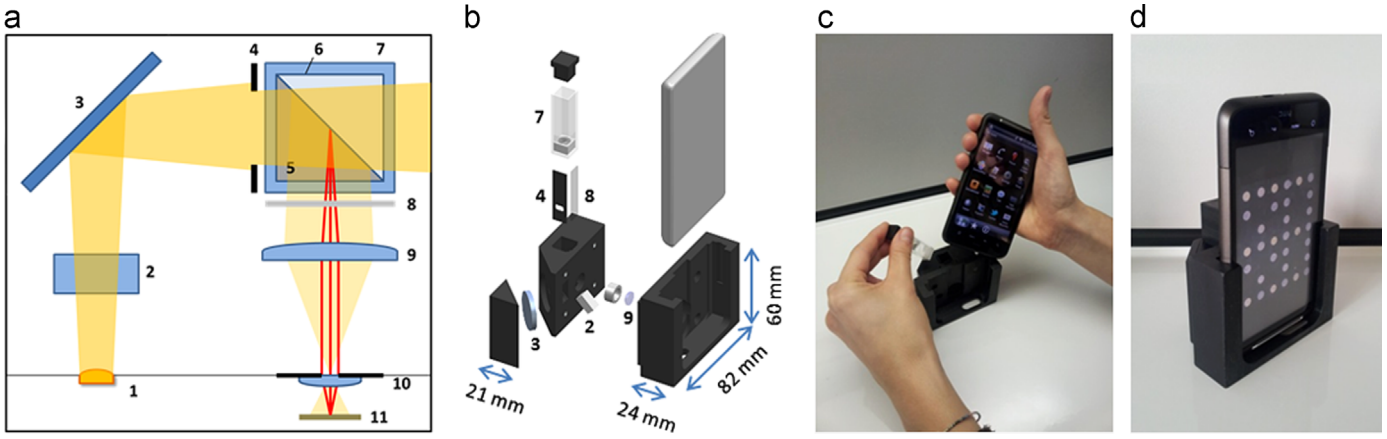

Fig. 1. Optical and mechanical schemes. (a) The optical elements contained in the plastic cradle to be attached to the phone are represented schematically. The light emitted by the phone flash LED (1) is brought to the same height of the camera sensor by means of a tilted glass window (2) and directed to the sample cell by a mirror (3). A diaphragm (4) selects the portion of light illuminating the sensing surface of the perfluorinated prism (5) in contact with the sample solution (6) contained in the measuring cuvette (7). The light reflected by the sensing surface passes through a polarizer (8) and a converging lens (9) and then impinges onto the phone camera hole, where one more converging lens is present (10), hence enabling the formation of an image on the image sensor (11). The incident and reflected light beams are represented as yellow shadows, whereas the red lines represent selected rays of reflected light showing the imaging conjugation with the detector plane. (b) Mechanical scheme of the plastic cradle, which is composed by three parts made of black polyoxymethylene, having the functions of holding the smartphone, the measuring cuvette, the magnetic stirrer and the optical components. The element numbers are the same as in panel (a). The magnetic stirrer (VarioMag-USA, Daytona Beach, FL, USA) has an approximate size of 12.5 mm x 12.5 mm × 5.8 mm and is inserted in the cradle 2 mm below the bottom of the cuvette. (c) Image of the assembled cradle during the insertion of the smartphone and the cartridge. (d) After filling the cuvette with an aqueous solution, the spotted sensing surface of the prism is imaged by the autofocus system of the phone and displayed on the screen, as shown in the picture. (For interpretation of the references to color in this figure legend, the reader is referred to the web version of this article.)

were covalently immobilized on the diagonal surface of the prism in 200-μm spots by means of an automated noncontact dispensing system (sciFLEXARRAYER S5; Scienion AG). After spotting, the prism was stored overnight in a humid chamber at RT. Afterwards, the unreacted NAS residues were blocked with a solution of 5% ethanolamine and washed with PBS Buffer. If required, the prepared prisms could be stored at 4 °C for at least 6 months with no apparent loss of function.

The sample cartridge was assembled by placing the prism into a 1-cm square cuvette hosting a plastic support containing a magnetic stir bar. In order to perform the measurement, the cuvette was inserted into the plastic holder and filled with about 0.8 ml of buffer solution (Fig. 1(c)) consisting of 0.15 M NaCl, 0.02% Tween 20, 1% BSA, and 0.05 M Tris · HCl, pH 7.6 (Sigma Aldrich). The serum experiments were carried out by adding 10% (vol/vol) of bovine fetal serum (Sigma Aldrich). The sample spikes were performed with 50 μl of buffer solution containing a variable concentration of target molecules.

A custom application running on the smartphone turned on the flash LED, acquired time sequences of the images of the light reflected by the sensing surface of the prism at 30 frame/s and displayed them in real time on the screen (Fig. 1(d)).

2.4. Data analysis

The subsequent analysis required a number of computational steps aiming at obtaining an accurate estimate of the unknown target concentration c in the sample solution. The processing steps include: (i) the conversion of the color images into 16-bit grayscale and the averaging of N consecutive frames (in this work $N=80$ or 150); (ii) the definition of a threshold-based mask enabling the localization of the spot regions in the images; (iii) the extraction of the average brightness as a function of time $u(t)$ for each spot and for the background area; (iv) the conversion of the $u(t)$ data into a variable $\Sigma(t)$ proportional to the surface density of bound material $\sigma(t)$; (v) the fitting of the $\Sigma(t)$ of each spot with exponential functions, from which (vi) the initial rate of increase of the adhering mass k_i is obtained from $d\Sigma/dt|_{t=t_0}$, where t_0 is the time of addition of the sample into the cartridge. In this study, the image sequence acquired by the smartphone was exported to a separate personal computer and the steps (i)–(vi) were performed by a Matlab script. However, the computational platform is assumed to be transitional since the whole analysis could be carried out by a suitable app running on the smartphone itself. Preliminary tests indicate that the most computationally demanding steps, (i) and (iii), can be executed by the smartphone on a single stack of 150 frames in less than two seconds, hence fast enough to enable the real-time processing of the acquired images during the measurement.

Step (iv) relies on the Fresnel laws of optical reflection, which in the case of a thin film separating two media with similar refractive index (Pedrotti et al., 2006) lead to the following equation (Giavazzi et al., 2013):

$$\Sigma(t)=\frac{\sigma(t)}{\sigma_0}=\sqrt{\frac{u(t)}{u_0}-1} \tag{1}$$

where u_0 is the brightness of the bare surface and σ_0 is a value that depends on the physical parameters of the system and represents the surface density yielding a twofold increase of the brightness relative to u_0. In the experimental condition here employed, $\sigma_0 \approx 4.9$ ng/mm^2 and $u_p/u_0 \approx 1.25$, where u_p is the brightness of the surface coated with the copoly(DMA-NAS-MAPS). Since the relevant interactions take place on the top of the spots, where few ng/mm^2 of antibodies are immobilized, the normalized surface density of target molecules $\Delta\Sigma(t)$ is obtained by subtracting the initial surface density of the spot from the measured $\Sigma(t)$. Given the small relative increase of the signal due to target binding on the top of the spot baseline, typically smaller than 30%, for each spot Eq. 1 can be linearized around the brightness value u_s measured before the addition of the target, hence obtaining the normalized surface density of target molecules on the top of the spot as:

$$\Delta\Sigma(t)\cong\frac{u(t)-u_s}{2\sqrt{u_0(u_s-u_0)}} \tag{2}$$

Eq. 2 also indicates that larger values of u_s, corresponding to larger amounts of antibodies immobilized in the spots, induces a more pronounced response of $u(t)$ to the binding of the target molecules.

3. Results and discussion

3.1. Multi-spot, label-free detection

Fig. 2 illustrates a test measurement performed on samples of IgG antibodies of different species (Rockland Immunochemicals, USA). Antibodies developed in mouse, guinea pig and rat were immobilized on the sensing surface in different spots. Fig. 2 (a) reports the image acquired by the smartphone set-up of a cell containing only the incubation buffer. The spots showed a rather different brightness, indicating, through Eq. 1, a different amount of immobilized probe antibodies. In this experiment, antibody samples of anti-mouse, anti-guinea pig and anti-rat IgG were added at different times, in order to evaluate the possible cross-interaction with the immobilized probes. The final concentration was 95 ng/ml for each target antibody in solution. The change in time of the measured spot brightness $u(t)$ is shown in the insets of Fig. 2(a). This experiment shows that a single spot provides a signal adequate for the analysis, whereas the comparison of the behavior of repeated spots located at different surface regions enables to estimate the intra-assay variability. Although, the initial value of reflected intensity differed from spot to spot within a factor of two, the increase measured at the end of the measurement is comparable—the range of the y-axis is kept constant in order to facilitate the comparison. Fig. 2(b) reports all the data shown in Fig. 2(a) converted into normalized surface density of target molecules, $\Delta\Sigma(t)$. Despite the different initial brightness, the binding curves measured from spots of the same species were remarkably similar and their fit with exponential functions (black curves) yielded relative standard deviations of the extracted rates of less than 5%. Moreover, Fig. 2(b) shows that the detection system enables to directly estimate the possible cross-interaction between antibodies of different species. A small increase of the spots brightness and of the corresponding $\Delta\Sigma(t)$ is observed as different targets were added in solution. The guinea pig spots provided a very small response to the addition of anti-mouse IgG and a slightly more pronounced effect was observed on rat spots when anti-guinea pig IgG were added. Overall, in this experiment, the estimate of the amount of antibodies binding on their partner spots is affected for less than 10% by the cross-interaction with untargeted antibodies.

3.2. Recovery of the binding curve in serum

As also shown previously (Giavazzi et al., 2013), the RPI detection method can be used to detect target proteins in a complex media such as serum, since the copoly(DMA-NAS-MAPS) strongly limits the unwanted, non-specific adhesion of the serum components on the sensing surface. In order to demonstrate the potential of the simpler smartphone-based device here proposed as a portable immunosensor, we performed experiments in a complex media (bovine fetal serum) aiming at the detection of viral proteins that are commonly used as biomarkers for the diagnosis of hepatitis B (hepatitis B surface antigen, HBsAg) and HIV (p24 capsid protein, p24Ag), provided by Dia.Pro Diagnostic Bioprobes, Italy. We addressed the measurement in the presence of serum with a twofold approach: the target proteins were added to the cuvette either about 1 h after (Fig. 3(a) and (b)) or at the same time (Fig. 3(c) and (d)) as the addition of the serum solution. Spots of antibodies targeting HBsAg (HBsAb, blue curves) and p24Ag (p24Ab, red curves) were prepared on the same chip. After filling the cuvette with a 1:10 dilution of serum without target molecules, the non-specific adhesion of serum components on the surface yielded an increase in the brightness of all spots, typically with a non-exponential behavior. After a couple of hours, the observed value of $\Delta\Sigma$ is about 0.07, which corresponds to a surface density of bound material of about 340 pg/mm^2, a value much lower than what was previously observed on a carboxyl-methyl-dextran coating in similar conditions (Giavazzi et al., 2013). Remarkably, the subsequent addition of a target recognized by the spotted antibodies yielded a relative response, on top of the serum signal, similar to that measured in buffer. Accordingly, the specific binding signal was obtained by subtracting the signal of reference spots, $\Delta\Sigma_R(t)$, substantially unaffected by the target addition, from that of the measuring spots, $\Delta\Sigma(t)$, hence obtaining a relative response $\delta\Sigma(t)=\Delta\Sigma(t)-\Delta\Sigma_R(t)$. In this proof-of-concept experiment, the spots targeting one test biomarker are used as the reference signal for the detection of the other. Indeed, the two antibodies, produced by the same manufacturer and from the same species, were selected to provide a very similar response to non-specific adhesion. In Fig. 3(a) and (c) the HBsAb spots provided the reference signal for the detection of p24Ag, and in Fig. 3(b) and (d) the p24Ab spots were used as reference for the measure of HBsAg. In each figure panel, the inset reports the recovered target binding curve after subtraction of the reference and its exponential fit. Remarkably, the simple subtraction proposed here led to similar binding rates in the two approaches, adding the serum previously and concomitantly to the target protein. However, when possible, even a preliminary partial equilibration of the sensing surface with serum before the addition of the target, as in Fig. 3(a) and (b), could potentially improve the robustness of the measurement, simply because the reference signal to be subtracted has a more limited curvature, and so a potentially smaller influence on the extracted binding rate.

3.3. A simple immunoassay format

Provided that the target binding curve could be recovered even in the presence of complex media, as described above, the use of the proposed immunosensor would require the estimate of an unknown target concentration from its binding signal. In principle, this could be performed by using an approach similar to the most used label-based assays, like ELISA, through the quantification of the amount of bound target at equilibrium (or at a certain time) and its comparison with a calibration curve performed at each measurement with a standard sample of known concentration. However, this approach, although very robust, is rather complex and highly time consuming, typically requiring trained personnel. Given the real-time capabilities offered by the proposed detection method, a procedure based on the kinetics of the binding reaction is feasible and could ideally eliminate the uncertainties due to the amount of binding sites available in each spot, without the need of a calibration curve at different concentrations. In this frame, an unknown concentration c could be in principle determined from the measurement of the association rate $\Gamma=ck_{on}+k_{off}$, where k_{on} and k_{off} are the association and dissociation kinetic constants of the binding reaction, where $K_d=k_{off}/k_{on}$ is the equilibrium dissociation constant. The extracted value of Γ can then be compared to the expected value for the particular interaction, with known kinetics constants. However, the procedure based on the extraction of the association rate has three potentially relevant limitations (Giavazzi et al., 2013): (i) a reliable measurement of association rate requires the observation of the binding curve for at least a time on the order of Γ^{-1}; (ii) for low values of c, $\Gamma\approx k_{off}$ and therefore the sensitivity at different concentrations is strongly reduced; (iii) in the absence of temperature control for the sample, the kinetics of the binding reaction could be affected by rather low reproducibility.

On the basis of these observations, a better approach for the smartphone device, in terms of robustness, sensitivity, dynamic linear range and time-to-result, could be arguably obtained simply

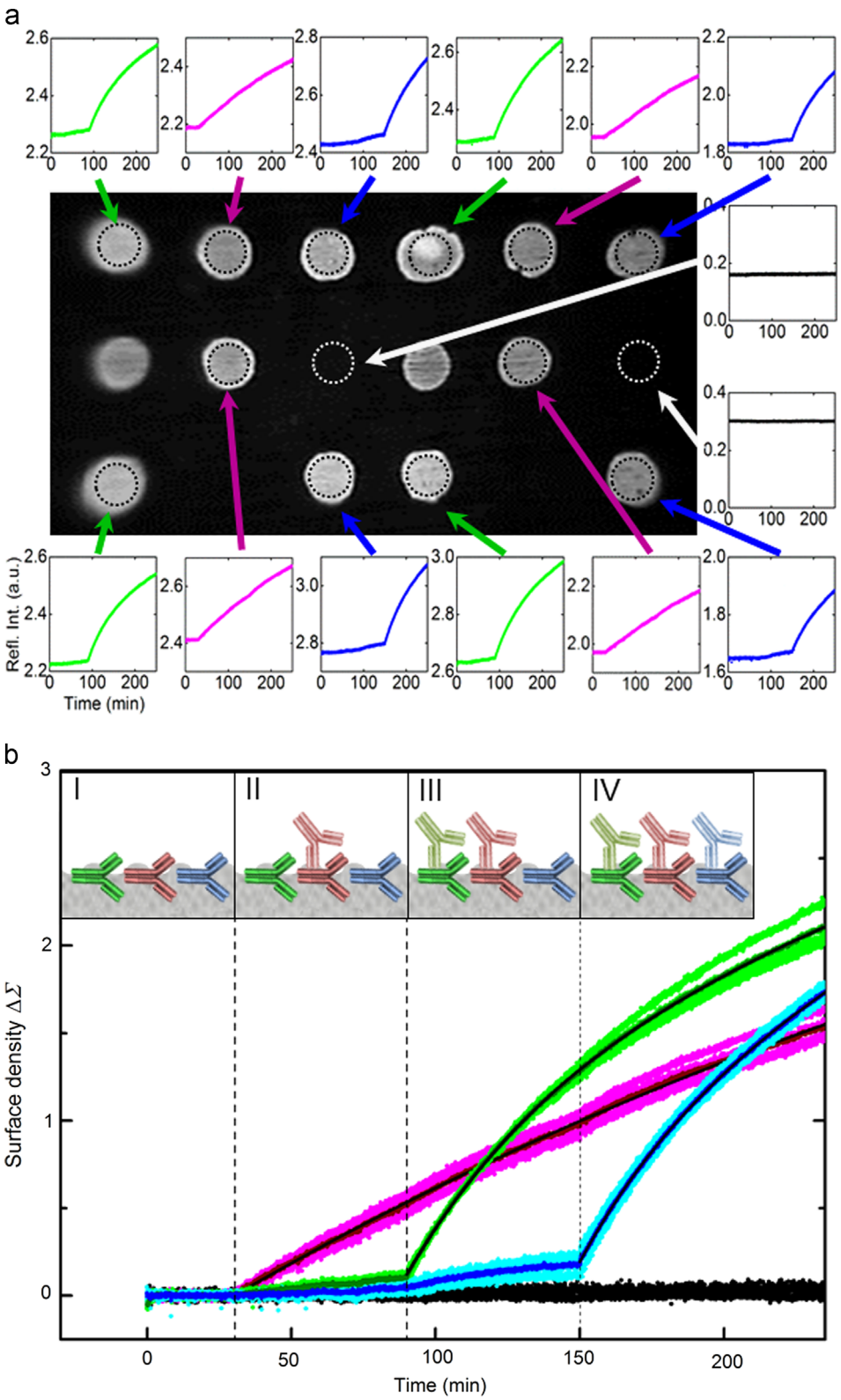

Fig. 2. Multiplex detection of IgG antibodies. (a) Image of a sensing surface with multiple spots of polyclonal IgG antibodies developed in different species and plots of the brightness as a function of time averaged on the surface regions indicated by the arrows and the dashed circles. The curves are color-coded according to the spotted antibody type: background (black), mouse (magenta), guinea pig (green) and rat (blue). Anti-mouse IgG were added at 30 min, anti-guinea pig IgG at 90 min and anti-rat IgG at 150 min. The change in time of the reflected light measured from a couple of unspotted regions are also reported. Each data point represents the average brightness of $N=150$ frames, corresponding to a point every 5 s. (b) The data shown in panel (a) are converted into the normalized surface density of material binding on the top of the spots $\Delta\Sigma(t)$ and reported with the same color-codes. The curves with corresponding darker colors represent the behavior averaged on all spots of the same kind, and the black curves are their exponential fits yielding rates of $2.01\times10^{-4}\,(\pm3\times10^{-6})\,s^{-1}$ (magenta), $8.31\times10^{-4}\,(\pm5\times10^{-6})\,s^{-1}$ (green) and $(9.87\times10^{-4}\,(\pm1\times10^{-5})\,s^{-1}$ (cyan). The times of the target additions are indicated as vertical dashed lines. Inset: the binding of the target antibodies in solution to the immobilized IgG is schematically represented before and after the additions (I–IV).

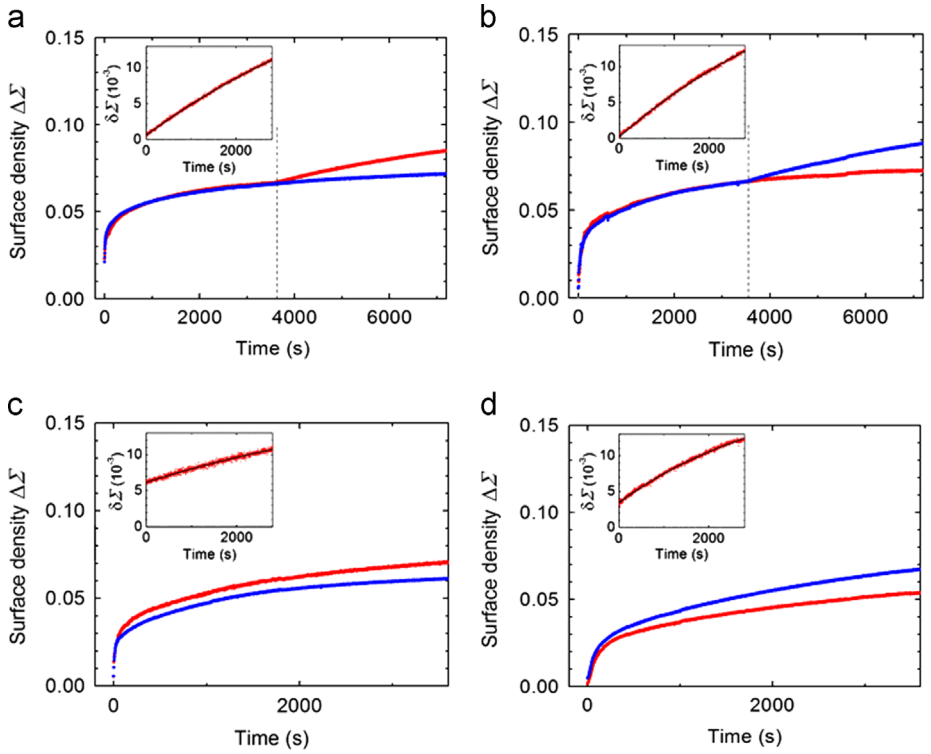

Fig. 3. Detection of HIV and hepatitis B markers in serum. The average surface density $\Delta\Sigma(t)$ on the top of four p24Ab (red points) and HBsAb (blue points) spots is shown after the addition of bovine fetal serum (1:10 dilution) at $t=0$ and subsequently of 76 ng/ml of p24Ag (a) or of HBsAg (b), at the time indicated by the vertical dashed lines. Similar experiments have been repeated adding the p24Ag (c) or the HBsAg (d) antigen at the same time of the serum (color codes are the same of panel (a) and (b)). Each data point represents the average brightness of $N=80$ frames, corresponding to a point every 2.67 s. Insets: relative increase $\delta\Sigma(t)$, obtained subtracting the HBsAb values from the p24Ab values (a and c) or the p24Ab values from the HBsAb values (b and d) of the corresponding main panel, reported as a function of the time after the antigen addition; the black lines represent exponential fits yielding rates of 1.6×10^{-4} ($\pm1\times10^{-5}$) s^{-1} (a), 1.9×10^{-4} ($\pm3\times10^{-5}$) s^{-1} (b), 1.5×10^{-4} ($\pm2\times10^{-5}$) s^{-1} (c) and 2.8×10^{-4} ($\pm3\times10^{-5}$) s^{-1} (d). (For interpretation of the references to color in this figure legend, the reader is referred to the web version of this article.)

focusing on the initial slope of the binding curve, which, different from the rate, always scales linearly with c. Accordingly, an unknown target concentration can be determined comparing the initial slope of the signal with that successively measured from the same spot after the addition of a standard sample with known concentration of the target (Fig. 4). In this case, different from the limitation in (i), the minimum time to perform the measurement is given by the time required to reliably detect a change of slope for a noisy signal. Indeed, the initial part of the binding curve expressed in terms of surface density of bound targets can be represented by a straight line as $\Delta\Sigma(t)=\Gamma_i t$, where $\Gamma_i=\Delta\Sigma_\infty k_{on}c$ and $\Delta\Sigma_\infty$ represents the normalized surface density reached at equilibrium for $c\gg K_d$, i.e. the value of $\Delta\Sigma$ that saturates the surface binding sites. In this respect, the detection of a change of slope would require to wait a time t_m, for which $\Delta\Sigma(t_m)\cong 3s$, where s represents the noise standard deviation. Thus, as opposed to limitation (ii), the minimum time-to-result is generally much shorter than Γ^{-1} and scales linearly with c^{-1} in any condition. In the experimental condition presented here, the standard deviation of the noise superimposed on the $\Delta\Sigma(t)$ signal is about 0.001 and, according to the results reported in Fig. 4, the minimum measuring time for a concentration of about 10 ng/ml of p24Ag could be less than 20 min, whereas the signal increase due to a concentration of about 180 ng/ml is determined in less than a minute.

A reliable quantification of target concentration in a sample can be obtained simply by adding in the same cuvette the reference sample with a known concentration. As reported in Fig. 4, the addition of the reference sample can be performed after a sufficient time to reliably estimate the slope of the signal following the addition of the measuring sample. In the case of relatively small increments of the signal due to the addition of the first sample, its target concentration can be simply obtained from the ratio between the slopes of the two curves. In the experiment shown in Fig. 4, the first target addition produced a linear increase of the signal, whereas the subsequent addition of a much higher concentration of target yielded an exponential response, from which the initial slope was derived through the fit with an exponential function. The measured slopes $d\Sigma/dt$ for the two curve fragments were 5.06×10^{-6} ($\pm2\times10^{-7}$) s^{-1} and 8.09×10^{-5} ($\pm1\times10^{-6}$) s^{-1}, being their ratio 16 ± 0.8, thus in good agreement with the value of 15.3 obtained as the ratio of the corresponding target concentrations, respectively. Ideally, an higher concentration for the reference sample would enable to perform a faster measurement, since, as previously discussed, the minimum observation time needed to determine the initial slope of the binding curve with a given accuracy linearly scales as c^{-1}. However, from one side limitations may arise from the finite frame rate of the image acquisition, and, on the other side, from the equilibration times associated with sample addition and mixing. The combination of these effects sets in less than a minute a reasonable lower bound for the observation time. Analogously, the same effects may limit the quantification of high concentrations of antigens. Considering a value of k_{on} of the order of 10^5 M^{-1} s^{-1}, as in the case of the p24Ab antibodies employed in this work (Giavazzi et al., 2013), the initial slope of the binding curves may not be accurately determined for concentrations higher than 10 μg/ml. Accordingly, given the linear dependence of the initial slope as a function of the antigen concentration and a detection limit of the order of ng/ml, the effective dynamic linear range of the proposed detection method extends for more than three orders of magnitude.

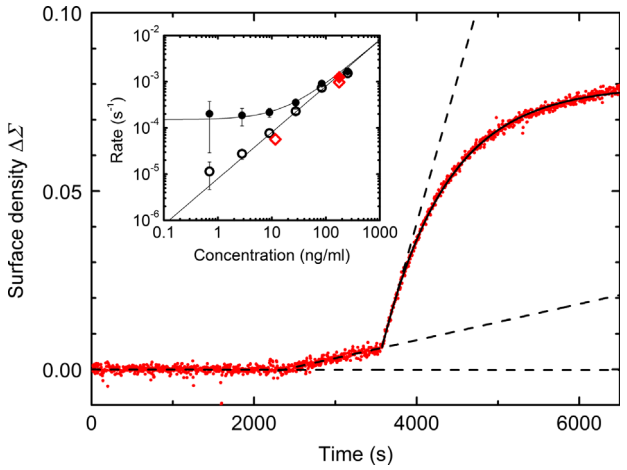

Fig. 4. Rapid quantification of target concentration. The surface density $\Delta\Sigma(t)$ on the top of a single spot of p24Ab is reported before and after two subsequent additions of p24Ag to final concentrations of 11.6 ng/ml and 177 ng/ml at 2295 s and 3575 s, respectively, in 1:10 dilution of bovine fetal serum. Each data point represents the average brightness of $N=150$ frames, corresponding to a point every 5 s. The black continuous line represents an exponential fit yielding a rate of 1.25×10^{-3} ($\pm1\times10^{-4}$) s^{-1}. The black dashed lines represent linear fits to the corresponding portion of the data yielding slopes $d\Sigma/dt$ of -2.6×10^{-8} ($\pm5\times10^{-9}$) s^{-1} (before the addition of the antigen), 5.06×10^{-6} ($\pm2\times10^{-7}$) s^{-1} (after the first addition) and 8.09×10^{-5} ($\pm1\times10^{-6}$) s^{-1} (after the second addition, slope extrapolated from the exponential fit). Inset: association rate (full black circles) and normalized initial slope $(1/\Delta\Sigma_\infty)\cdot d\Sigma/dt$ (open black circles) for the p24Ag/p24Ab interaction measured with the bench-top apparatus described in Giavazzi et al. (2013); each value represents the average rate obtained from six spots, and the error bars indicate the corresponding standard deviations; the surface density $\Delta\Sigma_\infty$ is obtained as the plateau value for $c\gg K_d$; the black lines represent linear fits with $\Gamma(c)=ck_{on}+k_{off}$ (association data) and $\Gamma_i(c)=ck_{on}$ (initial slope), from which the values of $k_{on}=14.4\times10^4$ ($\pm2\times10^4$) $M^{-1}s^{-1}$ and $k_{off}=14\times10^{-5}$ ($\pm2\times10^{-4}$) s^{-1} are obtained; the rate of the exponential fit and the normalized initial slopes reported in the main panel are represented as full and open red diamonds, respectively. (For interpretation of the references to color in this figure legend, the reader is referred to the web version of this article.)

3.4. Detection performance

Despite the minimal optical set-up, the consumer grade optoelectronics components and the absence of a temperature control system, the smartphone-based device can surprisingly reach overall performance comparable to that of the previously proposed, RPI bench-top apparatus (Giavazzi et al., 2013). In particular, two factors can be considered to affect mostly the detection performance of the device proposed here: (i) the capability of accurately measuring reproducible binding curves as a function of time; and (ii) the minimum amount of target molecules that can be detected on the top of the spots (i.e., the limit of detection, LOD). A preliminary observation supporting the property (i) is given by the experiment reported in the main panel of Fig. 4. Sequential additions of antigens delayed of about half an hour, induce signal changes consistent with the antigen concentration itself. Moreover, the binding curve at relatively high antigen concentration (180 ng/ml) is well described by a single exponential growth on a time interval of about 1 h. Considering that the temperatures of the sample and of the device are not controlled, these results are quite remarkable and support the intrinsic robustness of the method.

We also tested the property (i) comparing the kinetic parameter extracted from the experiment reported in Fig. 4 (main panel) with the results obtained for the same interaction using the bench-top apparatus. The inset of Fig. 4 shows that the slopes and exponential rates measured with the smartphone device (red dots) were in good agreement with the values extracted from the concentration dependence of the association curves measured by the bench-top apparatus, despite the different temperatures at which the two experiments were performed. The measurements with the smartphone device described here were performed at room temperature (about 23 °C ± 3 °C), whereas the temperature of the sample in the previously proposed bench-top system was held at 37 °C ± 0.1 °C. The high reproducibility of the extracted kinetics can be primarily ascribed to an accurate selection of the immobilized probe antibodies, chosen to minimize the temperature dependence of the binding parameters, and to the intrinsic robustness of the RPI method, operatively embedded into Eq. 1.

The LOD (ii) of the smartphone system can be estimated from the noise associated to the $\Delta\Sigma(t)$ signal, which turned out to be only slightly higher than that observed with the RPI bench-top apparatus. Indeed, the latter can potentially take advantage of an imaging sensor with lower background noise and of a light source with higher power and stability. From the data shown in the main panel of Fig. 4, it can be derived that the signal standard deviation s of $\Delta\Sigma(t)$ computed over a time interval of 2000 s represents about 1/80 of the saturation level of p24Ag reached at long times on the top of the p24Ab spot. The saturation value of $\Delta\Sigma=0.08$ can be converted into a surface density of about 390 pg/mm^2 through Eq. 1, thus the rms amplitude of the noise corresponds to about 5 pg/mm^2, a performance comparable to the best commercially available bench-top, label-free biosensors (Qavi et al., 2009) and, in particular, an unprecedented result with such a compact and simple to use device. It is shown that, through the proposed analysis based on the initial slope of the binding curve, such sensitivity enables to robustly detect 10 ng/ml of p24Ag in diluted serum in about 20 min. Considering the dilution factor of 1:10, the antigen concentration of a real sample of human serum would correspond in this case to 100 ng/ml. However, at that serum concentration the non-specific adhesion on plastic surface has almost reached the saturation level (Tsai et al., 1999). Therefore, the serum solution here employed can be assumed to be a rather good model also for the behavior of real samples with lower dilution. Moreover, further improvements are expected from pretreating the surface with suitable blocking agents capable of reducing the non-specific adsorption of serum components, hence possibly allowing the use of undiluted serum samples without a decrease of sensitivity.

A significant improvement of the detection limit is expected from the selection of antibodies with faster association kinetics. Since at low concentrations the slope of the binding signal linearly scales with the value of k_{on}, probe antibodies with particularly high k_{on} would provide a further reduction of the minimum detectable concentration in a fixed time. A theoretical limit is obtained considering that antibodies with k_{on} as high as $10^7\ M^{-1}\ s^{-1}$ are not uncommon. This value is about two orders of magnitude faster than that of p24Ab here employed (Giavazzi et al., 2013). Accordingly, an analogous decrease of the detectable concentration of p24Ag is expected, hence potentially enabling the detection of 100 pg/ml (about 4 pM) of antigen in about 20 min.

The performance of the proposed device can be evaluated in comparison to the ELISA method, the most common approach for human diagnostic tests. Many kinds of ELISA kits are commercially available for a huge variety of interactions, claiming very different detection limits, from pg/ml to μg/ml. Arguably, an analytical sensitivity of the order of 10–100 pg/ml is frequently observed. In particular, the antibodies used in this study are employed for the detection step in a sandwich ELISA kit claiming a sensitivity ≥ 100 pg/ml, therefore comparable to the theoretical detection limit of the device here proposed. As expected, being a label-free approach, the RPI method cannot compete with the most performing ELISA systems in terms of detection limit, whereas it features considerable advantages for what concerns operational simplicity, rapidity and dynamic range. The execution

of a pre-coated, sandwich format, ELISA test targeting a single molecular marker, typically requires at least 6 liquid handling operations to be repeated for many wells, including the addition of sample and reagents and the washing steps, hence involving the work of trained personnel in a furnished lab environment for about 3 h. Differently, the device here presented can execute multiplex detection of dozens of targets, only requiring a couple of pipette additions, possibly triggered by a suitable app running on the smartphone, with no washing or blocking steps and without requiring the generation of a standard curve at each measurement. The total execution time can be of about half an hour and, with the help of an appropriate software interface, there is no real need of specifically trained personnel. Therefore, the detection system proposed here offers great advantages in those conditions where the possibly lower sensitivities respect to the ELISA approach are not discriminating, and where simplicity, rapidity and multiplex detection are desired.

4. Conclusions

It has been previously shown that the RPI detection method enables the combination of good sensitivity with remarkable simplicity of the measurement procedure and instrument design. Here we have demonstrated a smartphone-based bio-sensing device with unprecedented easiness and rapidity, based on RPI. The proposed design exploits the flash LED, the camera sensor and, potentially, the computational power of the mobile phone, while a simple plastic attachment hosts a disposable cartridge containing the sensing surface, a tiny magnetic stirrer and few optical components. In the present set-up, the only external component is the stirrer driver, which, however, could be fully integrated into the device in a further engineering step and controlled by the phone through the USB port. The obtained assembled device is a portable, label-free biosensor with multiplex capabilities. As other, more complex instruments of the same class, it can be used to quantitatively characterize the interactions between surface immobilized probes and target molecules in solution. For this purpose, the addition of a suitable temperature control system would be preferable. Here we propose the use of the device also as a diagnostic tool with remarkable operational simplicity, requiring only two subsequent additions on the same cartridges to perform a multiplex measurements. As in any immuno-assay, the selectivity of the method depends on the performance of the probes (antibodies). Additionally, the imaging of multiple spots and their background provides a valuable tool to enhance the selectivity: The co-polymer surface regions and suitable antibody spots not interacting with the target molecules offer reference signals, through which the binding of the target can be recovered by subtraction. Moreover, the label-free detection approach, does not require the use of secondary antibodies, thus substantially avoiding the possible cross-interactions, which could affect the selectivity of label-based methods, when used in multiplex configurations.

A suitable app running on the smartphone could in principle perform all the analysis and provide estimates for the concentrations of dozens of biomarkers in the same sample of biological fluid (e.g., blood). Then, if needed, the results could be easily shared or transmitted to specialized personnel taking care of the diagnostic interpretation. Even if the sensitivity of the system is still not comparable to more complex, label-based laboratory techniques, which may detect concentrations as low as few pg/ml, the proposed device is expected to be of great interest for those situations in which rapidity, robustness, simplicity and multiplex detection have to be combined, such as in the case of screening of human diagnostic parameters in rough or poorly resource settings, for which current bio-sensing technologies are not adequate.

Acknowledgments

We thank Solvay Specialty Polymers R&D Center (Bollate, Italy) for providing the perfluorinated material and Dia.Pro Diagnostic Bioprobes (Milan, Italy) for providing the antibodies and antigens. This work was supported by the Cariplo Foundation (Grant 20069869), Italy and in part by EU (NAPES Project – NMP-2013-SMALL-7, project no. 604241).

References

Cretich, M., Pirri, G., Damin, F., Solinas, I., Chiari, M., 2004. Anal. Biochem. 332, 67–74.
Gallegos, D., Long, K.D., Yu, H., Clark, P.P., Lin, Y., George, S., Nath, P., Cunningham, B.T., 2013. Lab Chip 13, 2124–2132.
Ghetta, A., Prosperi, D., Mantegazza, F., Panza, L., Riva, S., Bellini, T., 2005. Proc. Natl. Acad. Sci. USA 102, 15866–15870.
Giavazzi, F., Salina, M., Cerbino, R., Bassi, M., Prosperi, D., Ceccarello, E., Damin, F., Sola, L., Rusnati, M., Chiari, M., Chini, B., Bellini, T., Buscaglia, M., 2013. Proc. Natl. Acad. Sci. USA 110, 9350–9355.
Gubala, V., Harris, L.F., Ricco, A.J., Tan, M.X., Williams, D.E., 2012. Anal. Chem. 84, 487–515.
Holford, T.R.J., Davis, F., Higson, S.P.J., 2012. Biosens. Bioelectron. 34, 12–24.
Huang, Y.-W., Ugaz, V.M., 2013. Analyst 138, 2522–2526.
Kozma, P., Lehmann, A., Wunderlich, K., Michel, D., Schumacher, S., Ehrentreich-Förster, E., Bier, F.F., 2013. Biosens. Bioelectron. 47, 415–420.
Lee, D., Chou, W.P., Yeh, S.H., Chen, P.J., Chen, P.H., 2011. Biosens. Bioelectron. 26, 4349–4354.
Morasso, C., Colombo, M., Ronchi, S., Polito, L., Mazzucchelli, S., Monti, D., Buscaglia, M., Bellini, T., Prosperi, D., 2010. Adv. Funct. Mater. 20, 3932–3940.
Myers, F.B., Lee, L.P., 2008. Lab Chip 8, 2015–2031.
Pedrotti, F.L., Pedrotti, L.M., Pedrotti, L.S., 2006. Introduction to Optics, third ed. Addison-Wesley
Prosperi, D., Morasso, C., Mantegazza, F., Buscaglia, M., Hough, L., Bellini, T., 2006. Small 2, 1060–1067.
Qavi, A.J., Washburn, A.L., Byeon, J.-Y., Bailey, R.C., 2009. Anal. Bioanal. Chem. 394, 121–135.
Tsai, W.B., Grunkemeier, J.M., Horbett, T.A., 1999. J. Biomed. Mater. Res. 44, 130–139.
Tseng, D., Mudanyali, O., Oztoprak, C., Isikman, S.O., Sencan, I., Yaglidere, O., Ozcan, A., 2010. Lab Chip 10, 1787–1792.
You, D.J., Park, T.S., Yoon, J.Y., 2013. Biosens. Bioelectron. 40, 180–185.
Zhu, H., Mavandadi, S., Coskun, A.F., Yaglidere, O., Ozcan, A., 2011a. Anal. Chem. 83, 6641–6647.
Zhu, H., Yaglidere, O., Su, T.-W., Tseng, D., Ozcan, A., 2011b. Lab Chip 11, 315–322.